the FEBS Journal

Structure/function analysis of spinalin, a spine protein of *Hydra* nematocysts

Simon Hellstern[1], Jörg Stetefeld[1], Charlotte Fauser[1], Ariel Lustig[1], Jürgen Engel[1], Thomas W. Holstein[2] and Suat Özbek[2]

1 Department of Biophysical Chemistry, Biozentrum, University of Basel, Switzerland
2 Institute for Molecular Evolution and Genomics, Im Neuenheimer Feld, Heidelberg, Germany

Correspondence
S. Özbek, Institute for Molecular Evolution and Genomics, Im Neuenheimer Feld 230, 69130 Heidelberg, Germany
Fax: +49 6221 545678
Tel: +49 6221 545638
E-mail: soezbek@zoo.uni-heidelberg.de

(Received 18 April 2006, accepted 18 May 2006)

doi:10.1111/j.1742-4658.2006.05331.x

The nematocyst capsules of the cnidarians are specialized explosive organelles that withstand high osmotic pressures of ≈15 MPa (150 bar). A tight disulfide network involving cysteine-rich capsule wall proteins, like minicollagens and nematocyst outer wall antigen, characterizes their molecular composition. Nematocyst discharge leads to the expulsion of a long inverted tubule that was coiled inside the capsule matrix before activation. Spinalin has been characterized as a glycine-rich, histidine-rich protein associated with spine structures on the surface of everted tubules. Here, we show that full-length *Hydra* spinalin can be expressed recombinantly in HEK293 cells and has the property to form disulfide-linked oligomers, reflecting its state in mature capsules. Furthermore, spinalin showed a high tendency to associate into dimers *in vitro* and *in vivo*. Our data, which show incomplete disulfide connectivity in recombinant spinalin, suggest a possible mechanism by which the spine structure may be linked to the overall capsule polymer.

Nematocytes are specialized cells in the phylum *Cnidaria*, harboring unique organelles called nematocysts. Nematocysts serve different functions such as capture of prey, defense and locomotion [1]. Despite the wide diversity of morphological types, all nematocysts have the same basic structure. They consist of a cylindrical capsule, surrounding a long coiled tubule, the wall of which is merged with the capsule wall and may be armed with spines, and an operculum. Capsule development takes place in a giant post-Golgi vacuole, in which the capsule wall is formed by the gradual addition of protein-filled vesicles from the Golgi apparatus. During this process, the external tubule is assembled at the apical end of the capsule and in a later stage invaginates into the capsule matrix and spines are assembled in the tubule lumen [2,3]. Finally, the wall hardens by a process involving disulfide polymerization of wall proteins [4–6], and the capsule matrix is filled with poly(γ-glutamate) (2 M), resulting in a high internal osmotic pressure of 15 MPa [7,8]. Major constituents of the nematocyst capsule in *Hydra* are members of the minicollagen protein family and the glycoprotein, nematocyst outer wall antigen (NOWA) [4,9,10]. Both proteins are believed to be involved in the hardening of the wall associated with disulfide polymerization caused by a switch from intramolecular to intermolecular disulfide bonds within their homologous cysteine-rich domains [4–6]. Upon mechanical stimulation, the mature nematocyst is able to discharge in an explosive process. Thereby the inverted tubule is everted and the spines are exposed to the outer surface.

The spines on the tubule surface have different functions depending on the nematocyst type, but all are presumed to have high mechanical strength. Stylets, the large spines of stenoteles, are needed to puncture

Abbreviations
FESEM, field emission scanning electron microscopy; NOWA, nematocyst outer wall antigen.

the cuticle of prey organisms when capsules discharge [1], while spines in desmonemes and isorhizas appear to function as barbs binding the discharged nematocyst to prey or to the substrate. Spinalin is a 24-kDa protein that is a constituent of spines and opercula of *Hydra* nematocysts [3]. Immunocytochemical analysis of developing nematocysts revealed that spinalin first appears in the matrix but is then transferred through the tubule wall at the end of morphogenesis to form spines on the external surface of the inverted tubule, and to form the operculum. Mature spines and opercula have lost their spinalin immunoreactivity, but it can be restored by mildly denaturing conditions. This indicates that spinalin is highly condensed in these structures [3].

Spinalin is not homologous to any protein in the databases, but has regions with partial homology to loricrins and keratins [3], which are also involved in forming structures with high mechanical strength. The spinalin primary sequence can be divided into four distinct regions following the putative signal peptide (Fig. 1A). At the N-terminus, it contains a large glycine-rich, histidine-rich region, which is presumed to form 'glycine loops'. This is followed by a putative polyglycine type II helical region, a lysine-rich region, and an acid tail at the C-terminus. Full-length spinalin could not be expressed in *Escherichia coli*, indicating that the protein is toxic for the host cells. A large fragment comprising regions I and II, but lacking the lysine-rich region and the acidic tail, could be overexpressed in *E. coli*. This N-terminal fragment was only soluble in buffer containing 2 M urea, and was used for the preparation of a polyclonal antibody [3].

In this study, we expressed full-length spinalin in a eukaryotic expression system using human embryonic kidney (HEK) 293 cells. The recombinant protein was soluble allowing for the first time a detailed structure/function analysis of full-length native spinalin. A structure-based homology screen revealed a similarity of the predicted spinalin structure to the toxin–agglutinin fold with extended flexible loops fixed by a four-disulfide core and forming a large dimerization interface.

Results

Detection of spinalin on discharged desmonemes by immunohistochemistry and field emission scanning electron microscopy (FESEM) analysis

To demonstrate the localization of spinalin on tubule structures of desmonemes, we performed immunohistochemistry and FESEM analysis of discharged capsules from *Hydra*. Figure 1B shows a desmoneme from a preparation of discharged nematocysts. Desmonemes represent a unique capsule type insofar as its tubule screws around an oblique axis during discharge giving it a corkscrew appearance. In contrast with the tubules of other capsule types, the twisted desmoneme tubule exhibits only one row of spines. Thus, during discharge the large spines of a desmoneme are placed inside the middle of the spiral-like tubule so that the bristles of a prey are firmly fixed. Immunocytochemistry revealed strong spinalin staining in the center of the everted coiled tubules (Fig. 1B). The capsule surface of the desmonemes showed only background staining intensity. FESEM analysis using protein A–gold confirms the localization of spinalin predominantly on the spines of the desmoneme tubule (Fig. 1C). Interestingly, the tubule surface showed some staining also. This may indicate that spinalin is integrated here in the tubule structure itself. Alternatively it may indicate rudimentary spines. The operculum was not labeled above the background level in all capsule types examined (not shown). This is consistent with immuno-

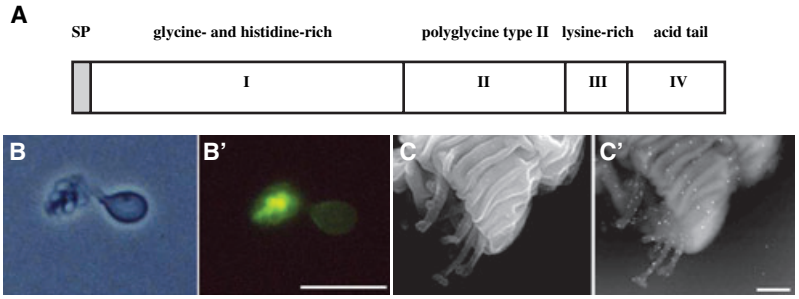

Fig. 1. Domain organization and localization of spinalin on discharged nematocysts. (A) Domain organization of spinalin. SP, signal peptide. (B) Overview of a discharged desmoneme visualized by immunofluorescence (B') and phase contrast microscopy (B). Scale bar = 20 μm. (C) Close view of the expelled tubule and spines of a desmoneme. Scale bar = 500 nm. (C') Electron micrograph visualizing the gold particles by back scattering.

fluorescence staining performed previously. Although spinalin is contained in nematocyst opercula, its accessibility is dramatically decreased during capsule maturation [3].

Expression and oligomerization of spinalin

A cDNA coding for full-length spinalin including the signal peptide was produced by PCR amplification, and an episomal expression vector was constructed to express the recombinant protein in EBNA-293 cells. Spinalin was secreted in a soluble form and detected in the cell supernatant by SDS/PAGE (Fig. 2A, lane 1). The previously described polyclonal antiserum against a bacterially expressed fragment of spinalin [3] specifically recognized the protein in crude cell culture supernatants (Fig. 2B, lane 1). FPLC on MonoQ resulted in strongly enriched spinalin preparations (Fig. 2A,B, lanes 2). The apparent molecular mass of the protein in SDS/polyacrylamide gels (Fig. 2A,B) was higher than that calculated from the protein sequence (28 kDa versus 23.7 kDa). However, analysis by ESI-MS revealed a mass of 23706.0 Da for the reduced protein (calculated mass of the reduced protein, 23 700.8 Da). The agreement between measured and calculated molecular masses showed that the difference between the apparent molecular mass of the protein in SDS/PAGE and the calculated one is not due to any post-translational modification. It also proves that the potential N-glycosylation site at position 243 at the acidic C-terminus of the protein is not occupied. MS of the nonreduced protein showed a mass of 23 700.0 Da. The difference between the molecular masses of the reduced and nonreduced protein indicates that several but not all of the eight cysteines of spinalin form internal disulfide bridges.

FPLC on MonoQ at pH 8.5 resulted in a spinalin peak eluted at 420–470 mM NaCl. This protein was used throughout this study if not otherwise mentioned. However, a second spinalin peak was often observed at 560–630 mM NaCl. SDS/PAGE in the absence of a reducing agent showed that the spinalin of the first peak migrates as a double band in the gel, with one band running at a similar position to spinalin in the reduced form, and the other band running slightly faster (data not shown), indicating that the spinalin sample contained proteins with two different oxidative states. Spinalin samples of the second peak from MonoQ FPLC did not enter the SDS/15% polyacrylamide separating gel in the absence of a reducing agent (Fig. 2A, lane 3), indicating that it forms large aggregates via disulfide bridges. Size exclusion chromatography on a Superose 12 column showed that this spinalin sample was eluted close to the exclusion volume of the column, which is 2000 kDa for globular proteins. Spinalin of both peak fractions was soluble in 20 mM Tris/HCl (pH 7.5)/150 mM NaCl (NaCl/Tris).

Recombinant spinalin was also investigated by transmission electron microscopy. Rotary shadowing of disulfide-linked polymeric spinalin (second peak from the FPLC on MonoQ) revealed aggregates of variable size (Fig. 2D). Many of these particles showed diameters between 20 and 30 nm, and thus consisted of more than 100 spinalin molecules. After reduction of the sample with dithiothreitol and alkylation of the cysteines with *N*-ethylmaleimide, particles of a homogeneous size were found (Fig. 2C). The protein was adsorbed to the mica surface at 1 μM, a concentration at which,

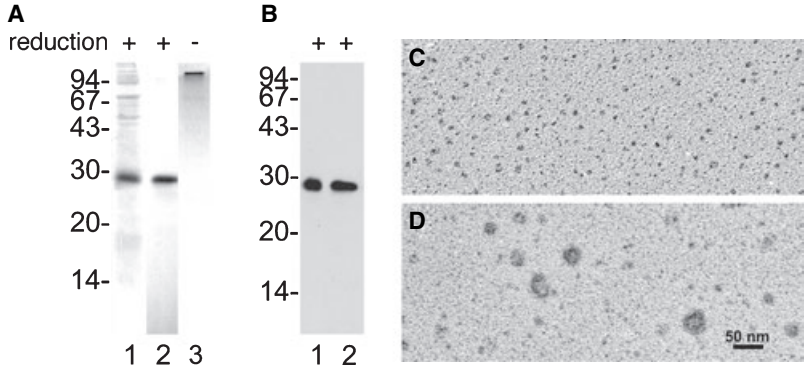

Fig. 2. Expression of spinalin in HEK293 cells and purification of the recombinant protein. Aliquots of serum-free culture medium of the cells (lanes 1) or of the protein purified by MonoQ FPLC (lanes 2) were subjected to SDS/PAGE (15% gel). Lane 3 shows a nonreduced sample of the aggregation peak eluted at ≈560 mM NaCl. Proteins were detected by Coomassie staining (A) or samples were analyzed by western blotting using spinalin antibody (B). Visualization of nonreduced aggregated spinalin (D) and reduced and alkylated spinalin (C) by electron microscopy after rotary shadowing. The scale bar indicates 50 nm and applies to both images.

according to ultracentrifugal analysis of the noncross-linked spinalin of the first peak, only monomers are present (Fig. 4A). The size of the particles is in agreement with this prediction, suggesting that the aggregation of spinalin of the second peak is mainly due to intermolecular disulfide linkages and not to hydrophobic interaction.

To investigate the cleavage of the proposed signal peptide, crude cell culture supernatants were treated with 10% trichloroacetic acid. The precipitated proteins were separated by SDS/PAGE and blotted on to poly(vinylidene difluoride) membranes. The spinalin protein band was excised and analyzed by N-terminal sequencing. The sequence obtained was RPWGPG, indicating that the protein starts at position 18. This finding is consistent with the proposed signal peptide comprising the first 17 amino acids of the protein [3].

Secondary structure of spinalin

The conformational state of spinalin was analyzed by CD spectroscopy and fluorescence spectroscopy. The CD spectrum of spinalin in NaCl/Tris showed a dichroic minimum centered at 205 nm (Fig. 3). The spectrum did not show the presence of pronounced α-helical or β-structures. This finding is consistent with the proposed domain organization of spinalin, consisting of four putative domains. The first domain is glycine-rich and histidine-rich and is presumed to form 'glycine loops'. It is followed by a putative polyglycine type II helical region, a lysine-rich region, and an acid tail at the C-terminus. Spinalin in 6 M guanidine hydrochloride showed a distinct reduction of the CD signal in the range 215–250 nm (Fig. 3). This reduction in secondary-structure elements suggests that the native protein is partly folded. This is also emphasized by fluorescence spectroscopy measurements. An excitation wavelength of 295 nm resulted in a red shift of the tryptophan fluorescence emission maximum from 340 nm in NaCl/Tris to 355 nm in 6 M guanidine hydrochloride (data not shown), indicating that the single tryptophan residue of spinalin in the N-terminal domain 1 is only partly exposed to the aqueous environment. Furthermore, at an excitation wavelength of 280 nm and in 6 M guanidine hydrochloride, the typical tyrosine fluorescence emission peak at 305–310 nm appeared, in contrast with the excitation in NaCl/Tris (data not shown). This result reveals that energy transfer from tyrosines to tryptophan occurs in the native protein in NaCl/Tris. Spinalin contains 14 tyrosine residues, 11 of which are located in domain 1, where the tryptophan residue is also located. This arrangement suggests that, at least within domain 1, energy transfer occurs from the tyrosine residues to the tryptophan residue.

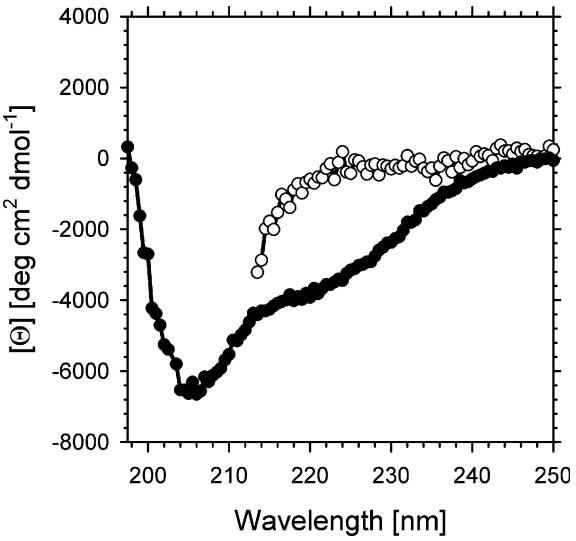

Fig. 3. CD spectra of native and denatured spinalin. Spectra were recorded at 25 °C. Native spinalin in NaCl/Tris (●) and denatured spinalin in 6 M guanidine hydrochloride (○) were used at protein concentrations of 15 and 3 μM, respectively.

Dimer formation of spinalin

Analytical ultracentrifugation was used for a more accurate analysis of the oligomeric state of soluble spinalin eluted in the first peak (Fig. 4A). At low protein concentrations (3 μM) in NaCl/Tris, sedimentation equilibrium experiments yielded an average molecular mass of 26 kDa, which is close to the calculated molecular mass of the monomer (23.7 kDa). Sedimentation equilibrium experiments were performed at concentrations up to 50 μM to see whether spinalin shows a tendency to self-associate at higher protein concentrations. The average molecular mass increased to 44 kDa at the highest protein concentration used, reflecting the formation of dimers. A plateau was clearly reached (Fig. 4A), indicating that specifically dimers, and not larger oligomers, are formed at higher protein concentrations. Spinalin that had been treated with 20 mM *N*-ethylmaleimide before purification on MonoQ to prevent oligomerization via disulfide bridges reached a similar plateau at ≈42 kDa in 20 mM Tris/HCl (pH 8.4)/430 mM NaCl (data not shown), and thus also specifically forms dimers at higher protein concentrations. The formation of dimers is therefore not dependent on the formation of disulfide bridges. Sedimentation velocity experiments at a protein concentration of 5.6 μM in NaCl/Tris (average molecular mass of 28.7 kDa; Fig. 4A) yielded a

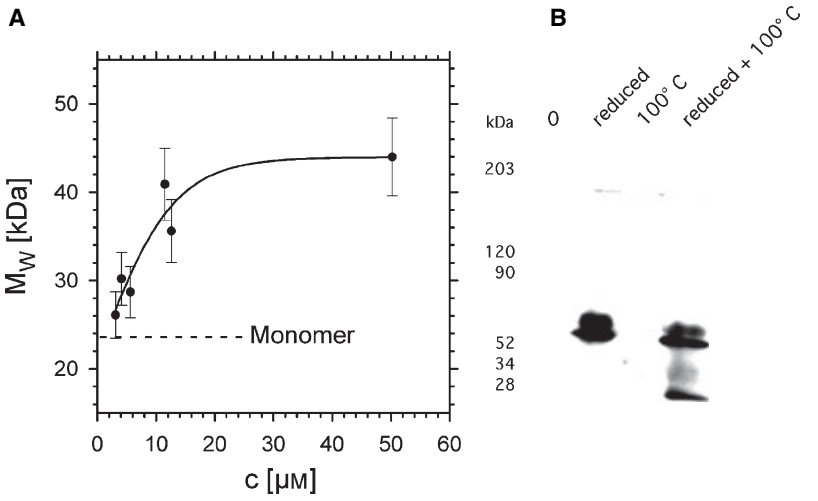

Fig. 4. Self-association of spinalin monitored by sedimentation equilibrium experiments and western blotting. (A) The change in the observed molecular mass as a function of the total monomer concentration is shown. Spinalin was measured in NaCl/Tris at 20 °C. The position of the monomer is indicated. (B) Identification of spinalin in extracts of nematocyst capsules treated with heat (100 °C) or reducing agents. Extracts were separated by PAGE (12% gel) and western blotted with spinalin antibody.

sedimentation coefficient of 2.1 S. The calculated frictional ratio f/f_0 was 1.4.

Spinalin was also found to form dimers in isolated nematocyst capsules. Figure 4B shows a western blot for spinalin in capsules submitted to SDS/PAGE analysis under different conditions. In samples that were not treated with reducing agent, no spinalin signal was detected indicating that the protein forms large disulfide-linked polymers that resist heat denaturation. Reduction without heating produced a double band at $\approx$ 55 kDa, which is consistent with the molecular mass of the dimeric protein. Reduction and heat denaturation converted parts of the dimeric spinalin to monomeric proteins with an apparent molecular mass of $\approx$ 26 kDa. This result points to much more stable dimer formation than found for recombinant spinalin, probably effected by additional post-translational modifications in *Hydra* cells.

Discussion

The cnidarian nematocyst is a unique organelle assembled from soluble precursor proteins that undergo a disulfide-dependent polymerization process during capsule maturation. Minicollagens and the glycoprotein NOWA, which are major constituents of the capsule wall, contain homologous cysteine-rich domains that are presumed to facilitate intermolecular disulfide bonding [6]. As most of the nematocyst structure can be dissociated by treatment with reducing agents, we assume that many nematocyst proteins are capable of participating in the disulfide network of the capsule structure. This capacity usually includes or even requires a disulfide-dependent self-assembly process, as in the case of NOWA [6]. Here we show that spinalin already forms large disulfide-linked aggregates during expression. As recombinant spinalin was partly monomeric, we assume that oligomerization may be a concentration-dependent process. Aggregation of spinalin was not found in samples treated with *N*-ethylmaleimide before purification (data not shown). Also, the aggregated protein fraction could be converted to monomers by reduction, indicating that oligomerization is facilitated by intermolecular disulfide bonds. The incomplete oxidative state of recombinant spinalin, as deduced from SDS/PAGE and MS, is in contrast with recombinant minicollagen-1 expressed in EBNA-293 cells [11]. This may point to an inherent structural disposition for intermolecular disulfide bonding. In mature capsules, spinalin was exclusively found in an insoluble oligomeric state. Treatment of capsules with reducing agent led to the release of soluble spinalin dimers that proved to be unusually stable. Even prolonged heat denaturation did not convert spinalin from nematocyst capsules quantitatively to monomers. This observation is in contrast with the behavior of the recombinant protein, which shows dimerization only at higher protein concentrations, and argues for a different post-translational modification or folding of spinalin in *Hydra* cells. We have made a comparable observation with recombinant minicollagen-1, which proved to have different triple helix stability from nematocyst minicollagen-1 [11].

To elicit structural features of spinalin, we performed sequence threading approaches (3DPSSM) [12], which revealed similarities of the putative 3D structure to the toxin–agglutinin fold [13]. Structural investigations of the wheat germ agglutinin [14] and several snake venom toxins [15–17] revealed domains folded into a series of coiled short loops linked together by four invariant disulfide bridges. The lack of secondary-structure elements is compensated in these domains by the strict

network of disulfide links. In the case of spinalin, subdomain I shows a pattern of several GYGG repeating motifs, which may provide the driving force for dimer formation, as stable dimers are retained after reduction with dithiothreitol. This hypothesis is supported by investigations of the C-type lectin rhodocetin [18,19]. Both heterodimeric subdomains in rhodocetin are formed by a conserved pattern of disulfide bridges stabilizing several loops. However, the interdomain interface is not stabilized via cystine formation, but by van der Waals contacts between several β-branched side chains (Leu81–Leu94 and Leu70–Leu90).

In future work, we will investigate how spinalin is integrated into the overall cysteine network of the capsule and which capsule proteins mediate its incorporation into the tubule structure.

Experimental procedures

Expression and purification of recombinant spinalin

The full-length spinalin cDNA sequence [3] was used as a PCR template to generate the cDNA construct for cloning. Oligonucleotide primers corresponding to the full-length sequence including the signal peptide were used: GAT CGGTACCATGGTGATCGCACAGGCTGC and GAT CCTCGAGTTATTAATCACCTCCATTTGGCATG for the 5′ and 3′ end, respectively. Sequences were verified by dye terminator cycle sequencing. They were inserted into the episomal expression vector pCEP-Pu [20] and used for transient episomal transfection of HEK cells that express the EBNA-1 protein of Epstein-Barr virus (EBNA-293 cells). Serum-free medium collected from cultures was centrifuged at 2500 ***g*** for 10 min and stored at −20 °C. To the harvested medium were added Tris/HCl, pH 8.4 or 8.5 (20–50 mM final concentration) and a mixture of protease inhibitors (1 mM phenylmethanesulfonyl fluoride, 1 μg·mL^{-1} leupeptin, 1 μg·mL^{-1} pepstatin final concentrations; in some experiments 1 μg·mL^{-1} aprotinin, 0.1 μg·mL^{-1} chymostatin, 0.5 μg·mL^{-1} leupeptin, 10 mM EDTA final concentrations). The medium was then passed through a 0.45-μm cellulose acetate filter. In some experiments, the solution was dialyzed against 20 mM Tris/HCl (pH 8.5)/120 mM NaCl or 20 mM Tris/HCl (pH 8.4)/1 mM EDTA and then centrifuged at 40 000 ***g*** for 20 min at 4 °C. The supernatant was applied to a 1-mL MonoQ FPLC column (Amersham Biosciences, Piscataway, NJ), the column was washed with 20 mM Tris/HCl (pH 8.5)/120 mM NaCl, and bound protein was eluted with 50 mL of a linear gradient from 120 mM to 1 M NaCl. In some experiments, the column was washed with 20 mM Tris/HCl, pH 8.4, and bound protein was eluted with 50 mL of a linear gradient from 0 to 1 M NaCl, or with 50 mL of a linear gradient from 0 to 0.4 M NaCl followed by 10 mL of a linear gradient from 0.4 to 1 M NaCl. Eluted spinalin was identified by SDS/PAGE and western blotting and dialyzed against NaCl/Tris. In some experiments, spinalin was dialyzed against 20 mM Tris/HCl, pH 7.5, followed by 10 mM Tris/HCl, pH 7.5, or was used without dialysis. Fractions with low concentration of spinalin were concentrated with Microcon YM-10 centrifugal filter devices (Millipore, Bedford, MA), and the protein was stored at −20 °C.

CD spectroscopy

An Aviv 62DS CD spectropolarimeter was used with thermostatically controlled 1-mm quartz cuvettes. Each spectrum was the average of two experiments with at least four scans, respectively. Buffer absorbance was subtracted using the filtrate of the buffer exchange step on Microcon YM-10 instead of the protein solution. The buffer used was 20 mM Tris/HCl (pH 7.5)/150 mM NaCl (NaCl/Tris). For the experiments with guanidine hydrochloride, the samples were diluted 1 : 4 with 8 M guanidine hydrochloride resulting in a final concentration of 6 M guanidine hydrochloride. The molar ellipticity (in degrees·cm^{-2}·dmol^{-1}) was calculated on the basis of a mean residue molecular mass of 110 Da. Measurements in the near-UV were hampered because of aggregation caused by the higher protein concentrations needed.

Analytical ultracentrifugation

A Beckman model XLA analytical ultracentrifuge equipped with absorption optics was employed. Sedimentation velocity runs were performed in 12-mm double-sector cells at 208 000 ***g***. Sedimentation equilibrium runs were performed using the same cells or using 4 mm cells but at a filling height of 2–3 mm only, and at rotor speeds of 17 600–44 220 ***g***. The measurements were performed in 20 mM Tris/HCl (pH 7.5)/150 mM NaCl or 20 mM Tris/HCl (pH 8.4)/430 mM NaCl at 20 °C. The molecular masses were calculated from sedimentation equilibrium runs using a floating baseline computer program that adjusts the baseline absorbance to obtain the best linear fit of ln$A$ versus r^2 (A is the absorbance and r is the distance from the rotor axis). A partial specific volume of 0.73 cm^3·g^{-1} was used for the calculations. The sedimentation coefficients were corrected to standard conditions (water at 20 °C).

Electron microscopy

Electron microscopy by the rotary shadowing technique was performed as described [21]. Reduction and alkylation of spinalin was performed by incubating the protein in 10 mM dithiothreitol followed by incubation in 25 mM *N*-ethylmaleimide (1 h at 37 °C for each step), and dialysis against 20 mM Tris/HCl, pH 7.5. Protein (10–100 μg·mL^{-1})

in 20 mM Tris/HCl, pH 7.5, was mixed with an equal volume of glycerol and sprayed on to freshly cleaved mica discs. These were dried in high vacuum, rotary shadowed with platinum/carbon at an angle of 9 °, and replicated.

Analytical methods

Protein concentration of spinalin was determined spectroscopically from the A_{280}, using a molar absorption coefficient of 26860 $M^{-1} \cdot cm^{-1}$ predicted from the amino-acid sequence [22]. The proteins were analyzed by SDS/PAGE as described by Laemmli [23]. For western blotting, the proteins were subjected to SDS/PAGE, transferred to nitrocellulose membranes (BA85, Schleicher & Schüll, Postach, Dasell, Germany), and analyzed with 1 : 2000 or 1 : 3000 diluted antiserum to spinalin [3] using the ECL detection system (Amersham Biosciences) to visualize bound secondary antibody on X-ray films. The spinalin antiserum used is identical with that applied by Koch *et al.* [3]. Nematocyst capsules were isolated from *Hydra vulgaris* tissue by elutriation as described previously [8]. Capsule integrity and the purity of the sample was confirmed by light microscopy. For analysis in SDS/PAGE, $\approx 10^5$ capsules were dissolved in Laemmli buffer with or without 2-mercaptoethanol and incubated at room temperature or 100 °C for 10 min.

Immunohistochemistry and FESEM analysis

Immunohistochemistry was performed as previously described [3]. For FESEM analysis, $\approx 1 \times 10^5$ capsules were suspended in NaCl/P_i and set on glass cover slides treated with polylysine. Capsules were then fixed with NaCl/P_i containing 0.2% glutaraldehyde and 2% formaldehyde for 10 min, subsequently rinsed for 10 min with 0.1 M phosphate buffer, pH 7.4, containing 2% BSA, and washed with 0.02 M glycine in NaCl/P_i. For immunogold labeling, capsules adsorbed to cover slides were blocked with 1% BSA in NaCl/P_i for 90 min at room temperature followed by incubation with antibody (1 : 50) and 15-nm colloidal gold-conjugated protein A in NaCl/P_i/1% BSA for 90 min each. Between each incubation step, capsules were washed several times with NaCl/P_i/1% BSA. Fixation was then performed with 2.5% glutaraldehyde in NaCl/P_i for 10 min. After several washing steps with NaCl/P_i, capsules were dehydrated stepwise with rising concentrations of ethanol (10–100%) before being subjected to critical point drying. FESEM analysis was performed in high-vacuum mode (10^{-5}–10^{-6} mBar) on a Phillips XL30 microscope.

Acknowledgements

We gratefully acknowledge the help of Alexander Koch with the cloning experiments. We thank Dr Paul Jenö for N-terminal protein sequencing and the ESI-MS experiments. We thank Sebastian Meier and Matthias Meier for performing CD measurements. This work was supported by the Swiss National Science Foundation (grant 31-49281.96 to J.E.).

References

1 Tardent P & Holstein T (1982) Morphology and morphodynamics of the stenotele nematocyst of *Hydra attenuata* Pall (Hydrozoa, Cnidaria). *Cell Tissue Res* **224**, 269–290.
2 Holstein T (1981) The morphogenesis of nematocytes in *Hydra* and *Forskalia*: an ultrastructural study. *J Ultrastruct Res* **75**, 276–290.
3 Koch AW, Holstein TW, Mala C, Kurz E, Engel J & David CN (1998) Spinalin, a new glycine- and histidine-rich protein in spines of *Hydra* nematocysts. *J Cell Sci* **111**, 1545–1554.
4 Engel U, Pertz O, Fauser C, Engel J, David CN & Holstein TW (2001) A switch in disulfide linkage during minicollagen assembly in *Hydra* nematocysts. *EMBO J* **20**, 3063–3073.
5 Ozbek S, Engel U & Engel J (2002) A switch in disulfide linkage during minicollagen assembly in hydra nematocysts or how to assemble a 150-bar-resistant structure. *J Struct Biol* **137**, 11–14.
6 Ozbek S, Pokidysheva E, Schwager M, Schulthess T, Tariq N, Barth D, Milbradt AG, Moroder L, Engel J & Holstein TW (2004) The glycoprotein NOWA and minicollagens are part of a disulfide-linked polymer that forms the cnidarian nematocyst wall. *J Biol Chem* **279**, 52016–52023.
7 Szczepanek S, Cikala M & David CN (2002) Poly-gamma-glutamate synthesis during formation of nematocyst capsules in *Hydra*. *J Cell Sci* **115**, 745–751.
8 Weber J (1990) Poly(gamma-glutamic acid)s are the major constituents of nematocysts in *Hydra* (Hydrozoa, Cnidaria). *J Biol Chem* **265**, 9664–9669.
9 Engel U, Ozbek S, Engel R, Petri B, Lottspeich F & Holstein TW (2002) NOWA, a novel protein with minicollagen Cys-rich domains involved in nematocyst formation in *Hydra*. *J Cell Sci* **115**, 3923–3934.
10 Kurz EM, Holstein TW, Petri BM, Engel J & David CN (1991) Mini-collagens in hydra nematocytes *J Cell Biol* **115**, 1159–1169.
11 Ozbek S, Pertz O, Schwager M, Lustig A, Holstein T & Engel J (2002) Structure/function relationships in the minicollagen of *Hydra* nematocysts. *J Biol Chem* **277**, 49200–49204.
12 Kelley LA, MacCallum RM & Sternberg MJ (2000) Enhanced genome annotation using structural profiles in the program 3D-PSSM. *J Mol Biol* **299**, 499–520.
13 Drenth J, Low BW, Richardson JS & Wright CS (1980) The toxin-agglutinin fold. A new group of small protein

structures organized around a four-disulfide core. *J Biol Chem* **255**, 2652–2655.
14 Wright CS (1977) The crystal structure of wheat germ agglutinin at 2–2 Å resolution. *J Mol Biol* **111**, 439–457.
15 Low BW (1976) Proceedings: structure studies of a sea snake neurotoxin 'erabutoxin b'. *J Biochem (Tokyo)* **79**, 27P.
16 Tamiya N & Takasaki C (1978) Detection of erabutoxins in the venom of sea snake *Laticauda semifasciata* from the Philippines. *Biochim Biophys Acta* **532**, 199–201.
17 Tsernoglou D & Petsko GA (1976) The crystal structure of a post-synaptic neurotoxin from sea snake at A resolution. *FEBS Lett* **68**, 1–4.
18 Eble JA, Beermann B, Hinz HJ & Schmidt-Hederich A (2001) alpha 2beta 1 integrin is not recognized by rhodocytin but is the specific, high affinity target of rhodocetin, an RGD-independent disintegrin and potent inhibitor of cell adhesion to collagen. *J Biol Chem* **276**, 12274–12284.
19 Paaventhan P, Kong C, Joseph JS, Chung MC & Kolatkar PR (2005) Structure of rhodocetin reveals noncovalently bound heterodimer interface. *Protein Sci* **14**, 169–175.
20 Kohfeldt E, Maurer P, Vannahme C & Timpl R (1997) Properties of the extracellular calcium binding module of the proteoglycan testican. *FEBS Lett* **414**, 557–561.
21 Engel J (1994) Electron microscopy of extracellular matrix components. *Methods Enzymol* **245**, 469–488.
22 Pace CN, Vajdos F, Fee L, Grimsley G & Gray T (1995) How to measure and predict the molar absorption coefficient of a protein. *Protein Sci* **4**, 2411–2423.
23 Laemmli UK (1970) Cleavage of structural proteins during the assembly of the head of bacteriophage T4. *Nature* **227**, 680–685.